ABSENCE OF COUNTER SPIRALS IN BASILISK NUMERICAL SIMULATIONS

Ishaan Kakadé

Stéphane Perrard

École Polytechnique - LadHyx

September 2018

Contents

Abstract

The purpose of this document is to summarize the numerical simulations carried out using open source code - Basilisk (written in C); developed by S. Popinet and post-processed in MATLAB with a focus on the numerical implementation and corroboration with known physical laws and experimental observations. Within the frame of Basilisk's Navier-Stokes equation solver, no counter spirals are post-processed. The work presented here is intended to serve as a guide to any authorized individual trying to run the simulation, perhaps with different physical parameters as well as to show the capabilities of the code package.

1 Introduction

Various analytical and experimental studies have been carried out with regard to gravito-capillary waves in past. The propagation of these gravito capillary waves is of particular importance to the study of the Whirligig beetle (Gyrinidae), a species of insect that lives on the water-air interface and whose circular motion produces surface propagating gravito-capillary waves. The motion of this insect is simulated using a moving pressure source which is moved in a uniform circular trajectory on a fluid-air interface.

The numerical simulations were carried out using the software Basilisk (written in C) developed by S. Popinet for fluid dynamics numerical simulations. The centred Navier-Stokes solver of Basilisk and a volume of fluid method to were used to simulate two phase flows accurately. An additional module is used to take surface tension effects into account. First, the numerical accuracy was tested by looking at the dispersion relation of 'gravito-capillary' waves using stationary waves in a 2 dimensional space. Then additional functions were implemented to apply inter facial forces that can vary in space and in time. Still in the 2 dimension of space configuration, two cases were studied:

1. Asymptotic interface shape under Gaussian pressure source using high viscosity fluid.
2. Temporal response of the interface to a pressure source moving at constant speed using low viscosity fluid.

Then, full 3D simulations were carried, still using the centred Navier-Stokes solver of Basilisk. Here too, 2 cases were studied:

1. Asymptotic interface shape under Gaussian pressure source using high viscosity fluid.
2. Temporal response of the interface to a pressure source moving in constant circular motion in water.

In all the simulations, the Basilisk solver was used and MATLAB was then used to post-process and visualize the output data.

2 Dispersion Relation Analysis

A dispersion relation analysis was carried out to observe the trend of the phase velocity with respect to a dimensionless wave number (kLc) and to verify its conformity with theoretical curves. The graphs are thus obtained by sweeping across the dispersion relation by varying the surface tension of the liquid and calculating the period of the resulting wave after an initial cosine wave is placed at the interface. Figures 1 to 6 outline the various results obtained from the dispersion relation analysis. Here the capillary length, Lc, is the relevant length scale. Numerically, we vary the restoring force of the interface by changing the dimensionless wave number 'kLc' through a variation in the value of surface tension.

As in the standard dispersion relation, values of kLc that are much smaller than 1 represent pure capillary waves and values of kLc that are much greater than 1 represent pure gravity waves and around kLc =

1, both effects are non-negligible, causing the aforementioned 'gravito-capillary' waves. The dimensionless analytical dispersion relation is presented in equation. 1 and is plotted in red in Fig. 2 and Fig. 3

$$c = \frac{1}{2\pi}\sqrt{\left(\frac{1 + kLc^2)}{kLc}\right)} \tag{1}$$

Where, c is the phase velocity, k is the wavelength and Lc is the capillary length.

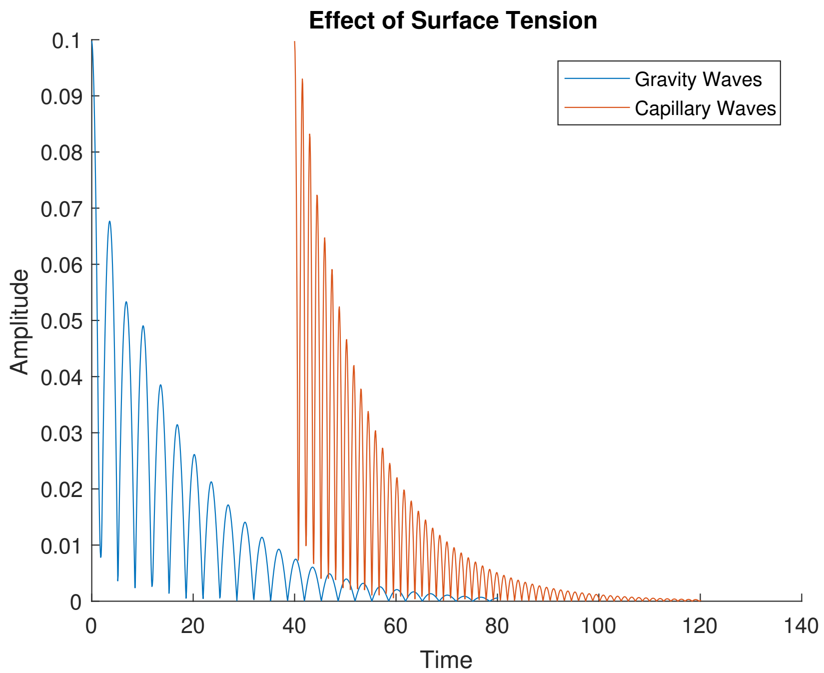

Figure 1: Increased surface tension increases the frequency of the wave as seen here with a lower surface tension on the blue gravity wave and a higher surface tension on the red wave.

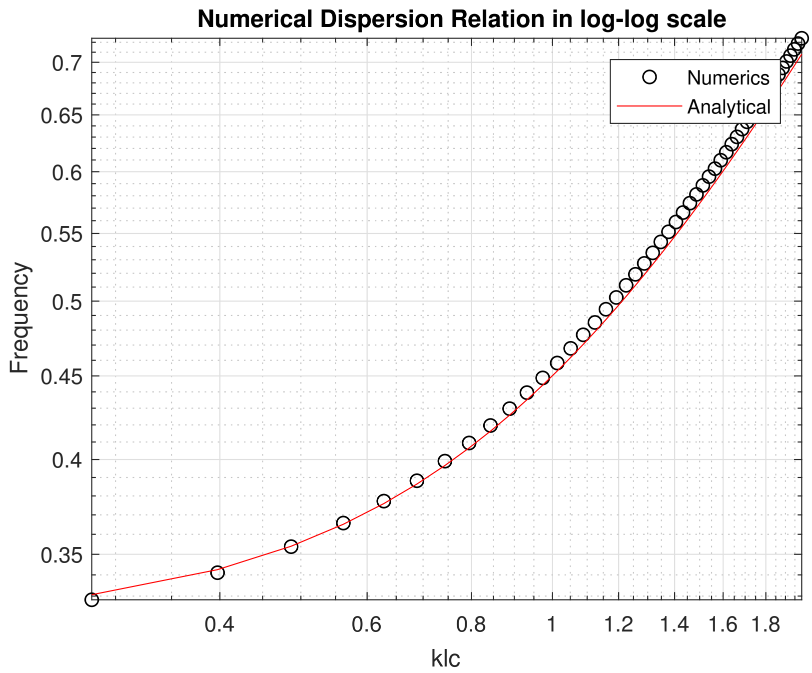

Figure 2: Frequency dispersion across kLc showing an increase in frequency with an increase in the value of kLc and in close correlation with analytical results

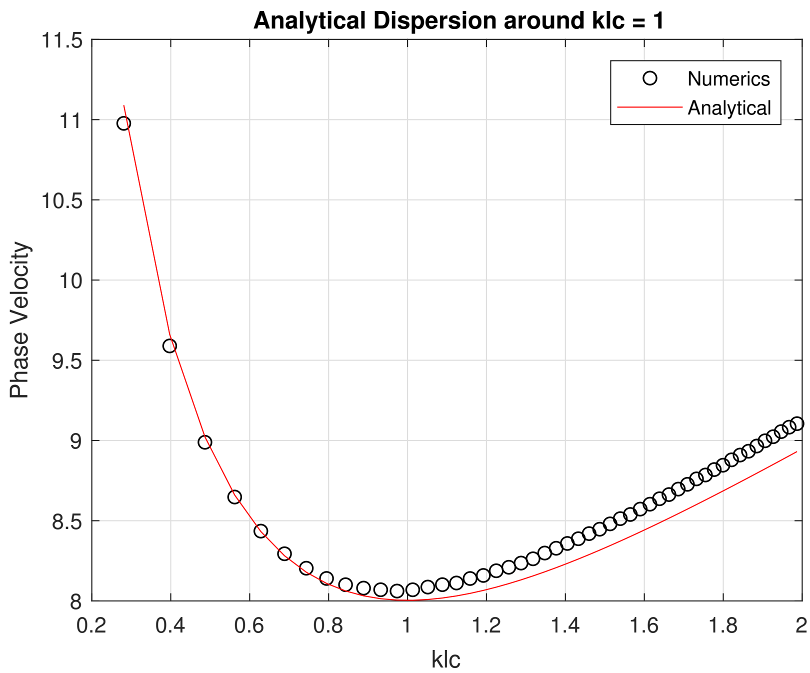

Figure 3: Dispersion of phase velocity across around kLc = 1 showing close correlation with analytical curve plotted from equation. 1.

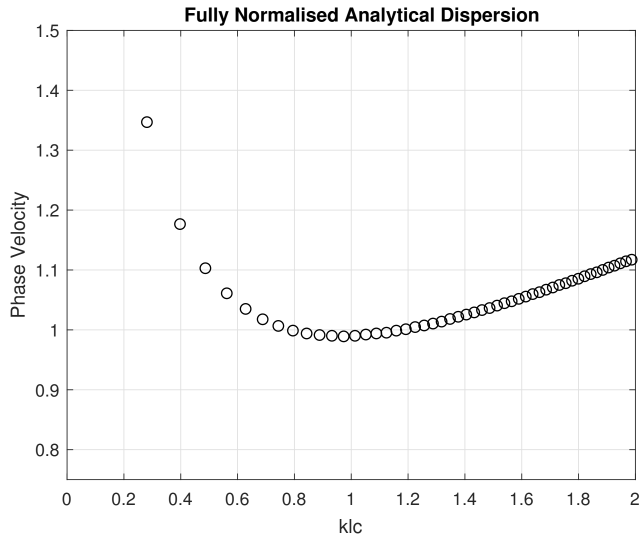

Figure 4: Full normalized dispersion relation where the phase velocity is normalized with the minimum phase velocity and kLc is already dimensionless showing an a minimum almost at (1,1).

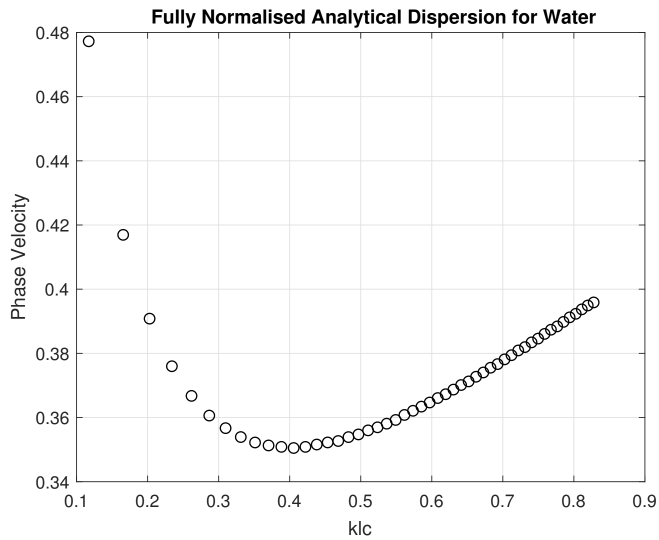

Figure 5: Full normalized dispersion relation for water with a minimum at 1/kLc.

3 Application of Static Pressure Source in 2D

As seen in Fig. 6, the blue curve represents the liquid interface while the red curve is the applied Gaussian inter facial pressure. To prove that this inter facial force represents true physics, the applied pressure force should be balanced by hydro static forces within the liquid as in equation (1) and this tends to be the case as seen in Fig. 8 where the maximum amplitude of the deformed interface reaches a maximum value and then stabilizes at a particular depth of penetration. The curve has this particular shape as the the high viscosity liquid is over damped, and does not allow an oscillation of the interface.

$$\rho_l g \xi(x) = P(x) \tag{2}$$

Where, rho is the density of the liquid, g is the acceleration due to gravity, xi(x) is the profile of the interface deformation.

Numerically, an inter facial force is applied using the reduced gravity approach of the Basilisk solver by modifying the value of the 'height function' of the interface based on a user defined inter facial force. This required a modification of the 'position' function of the Basilisk solver. Using a curve fitting function in MATLAB, and comparing the equations' coefficients, a close correlation is observed between the shape of the applied pressure and the shape of the interface in the static state as seen in equation (2) of the applied pressure force shape and equation (3) of the interface deformation shape acquired from the curve fitting on MATLAB.

$$P(x) = -exp(\frac{x-10}{0.5})^2 \tag{3}$$

$$\xi(x) = -1.004exp(\frac{x-10}{0.648})^2 \tag{4}$$

The differences between the curves may be explained by the fact that interface shape is slightly changed due to the finite dimensions of the box and that the conservation of mass pushes the level of water up by a certain height, thus changing the shape of the surface deformation across the box.

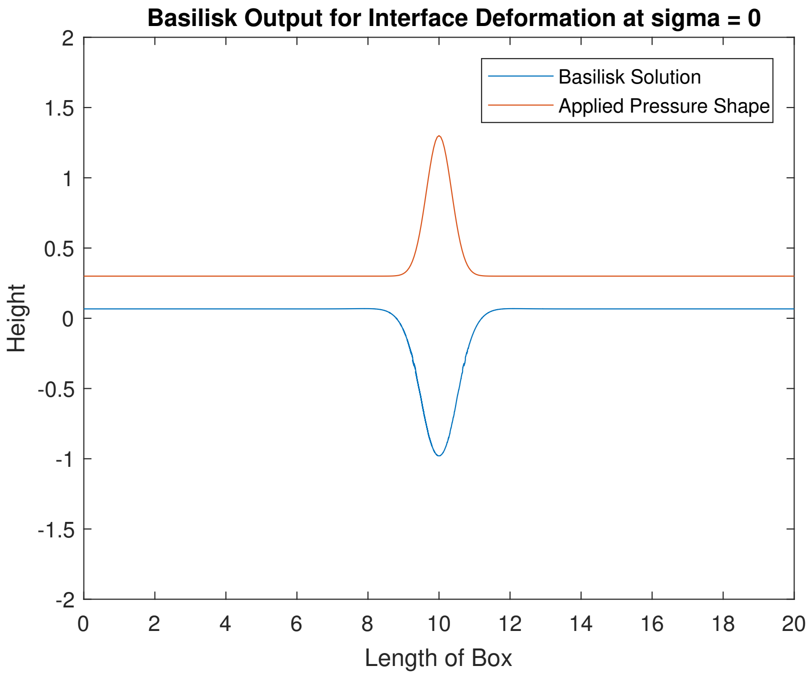

Figure 6: Static pressure (in red) applied on a high viscosity liquid interface (in blue) after applying a force for a numerical time of 20 seconds.

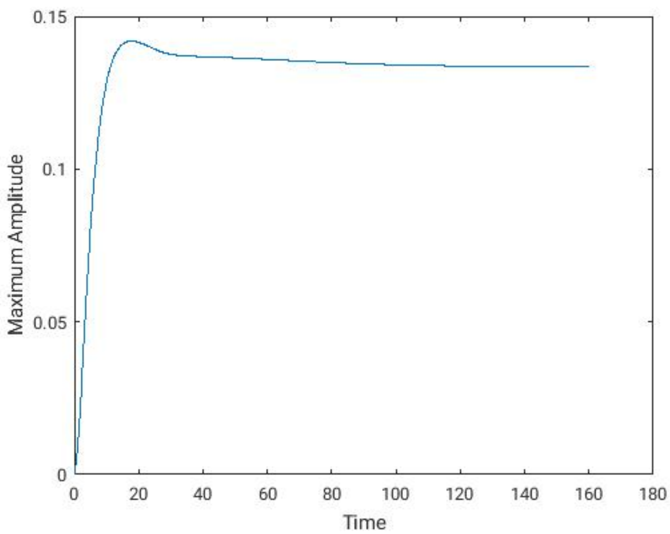

Figure 7: Evolution of maximum depth of penetration by the pressure force over time is asymptotic.

3.1 The Bond Number

Given the play between surface tension and gravity as the driving force behind the waves, it proved noteworthy to evaluate the Bond number (Bo) and compare it to the depth of penetration and, as expected, the depth of the penetration decreases rapidly with a decrease of bond number and increases as bond number increases. The characteristic length is taken to be the width of the applied pressure force. This can be seen mathematically from the equilibrium equation for a static meniscus shown below:

$$P(x) = \rho g h(x) - \sigma \Delta h \tag{5}$$

By replacing surface tension by its equivalent capillary length and making the equation dimensionless in the Fourier space, a set of terms corresponding to the Bond number appears.

$$\frac{\widehat{P(x)}}{\rho g \widehat{h(x)}} = 1 + \frac{2\pi}{B_o} \tag{6}$$

Where, Bo $= \rho g a^2/\sigma$

Here, the width of the Gaussian pressure distribution, 'a', is taken as the characteristic length for the Bond number.

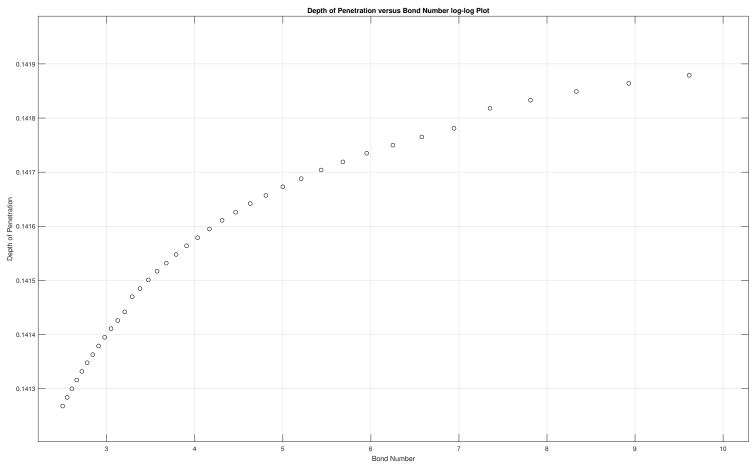

Figure 8: Bond number versus depth of penetration at the interface in log-log scale.

3.2 Effect of Surface Tension

As the surface tension is increased, the imprint of the static pressure source is reduced in terms of maximum penetration. These effects are visualized in Fig 9 and Fig. 10.

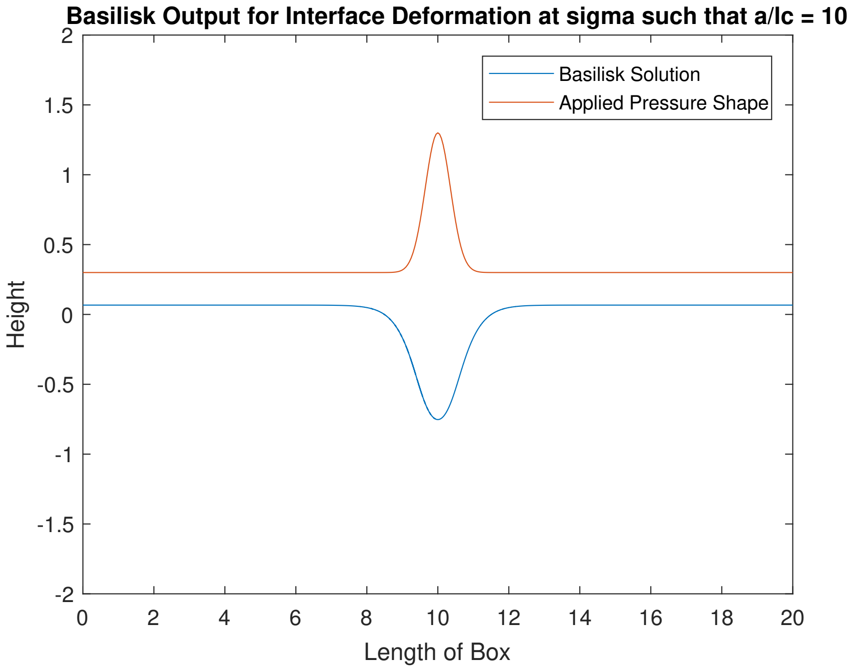

Figure 9: Static pressure imprint on liquid interface with lower surface tension.

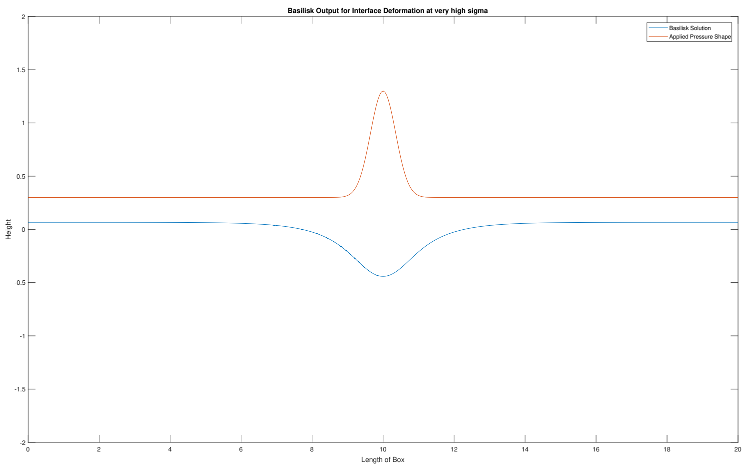

Figure 10: Static pressure imprint on liquid interface with higher surface tension.

4 Application of Moving Pressure Source in 2D

4.1 Qualitative Simulation Results

By adding a time dependency to the centre of the Gaussian distribution of the pressure source, the source was moved across the interface (left to right) at different speeds and the kinds of waves were qualitatively observed during post processing and it may be observed in Fig. 11 and Fig. 12, that at low speeds of the moving source (0.2m/s), none or minute wave generation is seen in bow or aft of the source but as the speed was increased, a higher frequency wave is generated in the aft of the moving pressure source compared to the wave generated in the bow of the pressure source. As speed was further increased, these two frequencies diverged further.

Numerically, the speed was raised by increasing the parameter 'S', which is directly proportional to the rate at which the source moves across the interface in meters per second. The animation of these simulations is presented in the files S0.1.gif to S1.gif, attached with this package.

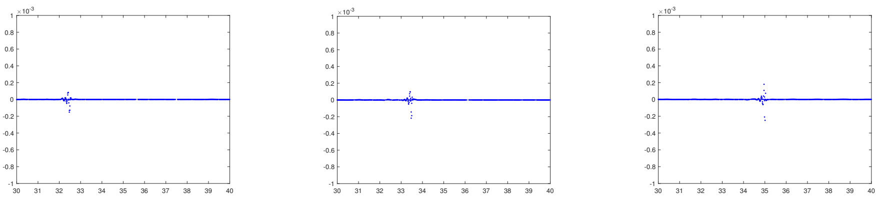

Figure 11: Snapshots of a moving pressure inter-facial force moving from the left to right at 0.1m/s produced close to no surface waves.

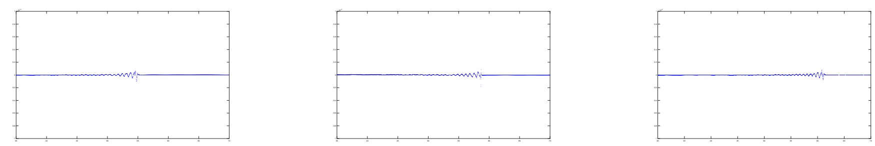

Figure 12: Snapshots of a moving pressure inter-facial force moving from the left to right at 1m/s producing far field surface waves.

To conduct a temporal analysis, two height probes are placed as seen in Fig.13. These probes are like floaters and will provide the level of the interface as the waves pass by them. The response of the height probes are visualized in Fig. 14 to Fig. 18.

Note: Given that the signal is noisy, a Fourier analysis needs to be conducted to parse through the signal in the frequency domain and determine the frequency of the main waves, aft and bow.

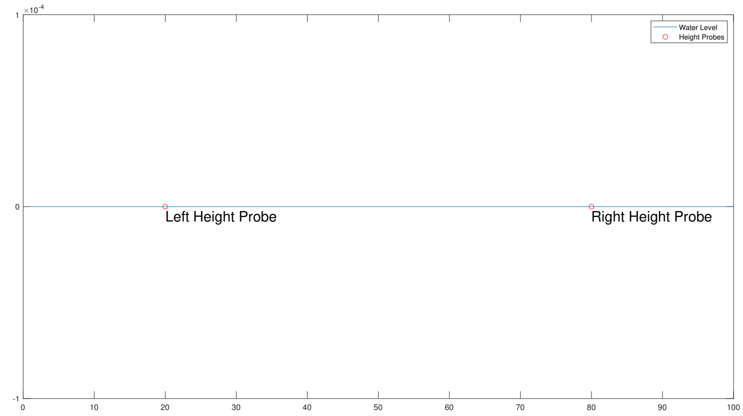

Figure 13: Position of height probes (Red) on the water surface (Blue) used for the temporal analysis

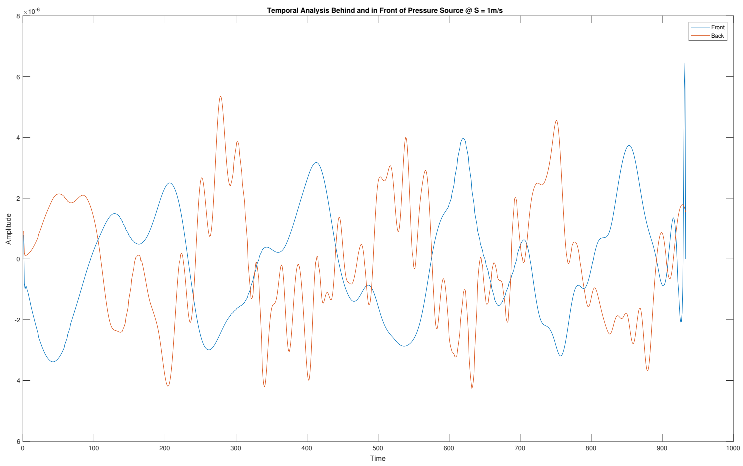

Figure 14: Height probe readings using a faster moving pressure source (moving from left to right) with higher frequency at the aft (Red) of the source and lower frequency at the bow (Blue) of the source, speed S = 1m/s.

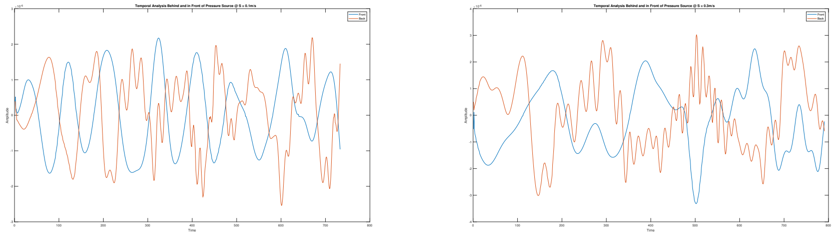

Figure 15: L-R: Height probe readings with speed of moving pressure source - S = 0.1 m/s and S = 0.3m/s

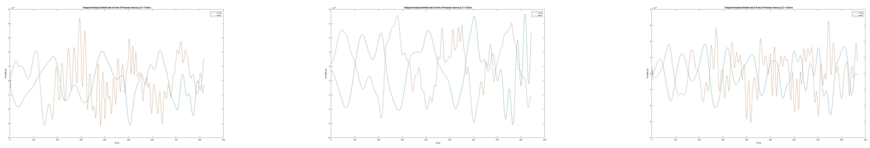

Figure 16: L-R: Height probe readings with speed of moving pressure source increased from S = 0.4 m/s to S = 0.6m/s

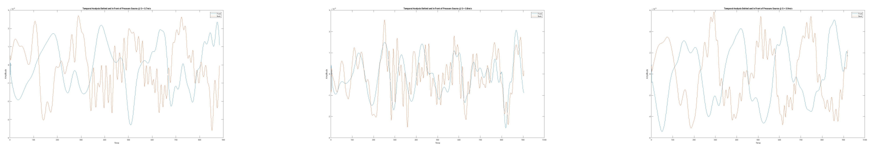

Figure 17: L-R: Height probe readings with speed of moving pressure source increased from S = 0.7 m/s to S = 0.9m/s

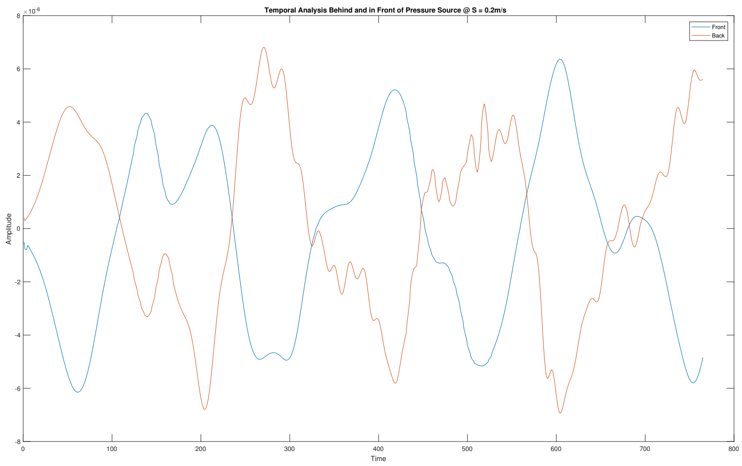

Figure 18: Height probe readings using a moving pressure source (moving from left to right), speed S = 0.2 m/s where the waves on either side of the moving pressure source are similar.

4.2 Quantitative Simulation Results

The following analysis was conducted similar to the one conducted in section 4.1, using height probes but rather than looking at far field waves, we look at the frequency of the wave closer to the moving pressure at a particular time step while varying its speed. By such a process, figures like Fig. 19 were plotted and analyzed and the corresponding graphs are presented in Fig. 20 through Fig.22. Waves of a very similar frequency are observed on either side of the pressure source, in accordance with the theory when the phase velocity is minimum for water.

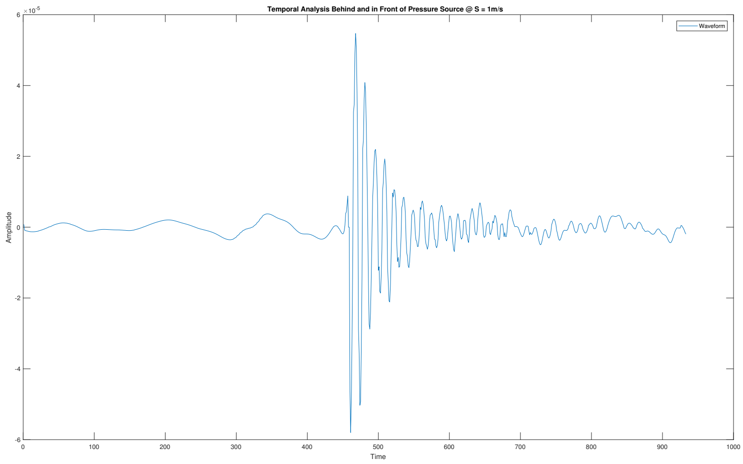

Figure 19: Temporal analysis with a height probe fixed at a single point with the pressure source sweeping past it at half of the total time of simulation at 1m/s.

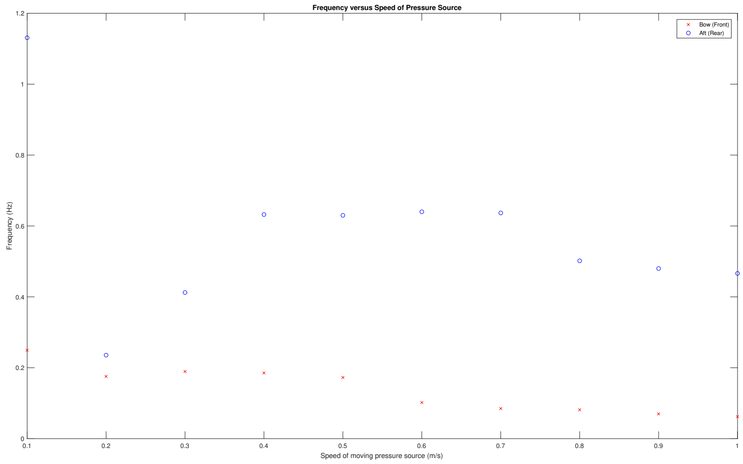

Figure 20: As predicted by the dispersion relation, for a minimum phase velocity, only a single solution for the wave number exists; for water the minimum phase velocity is approximately 0.2m/s

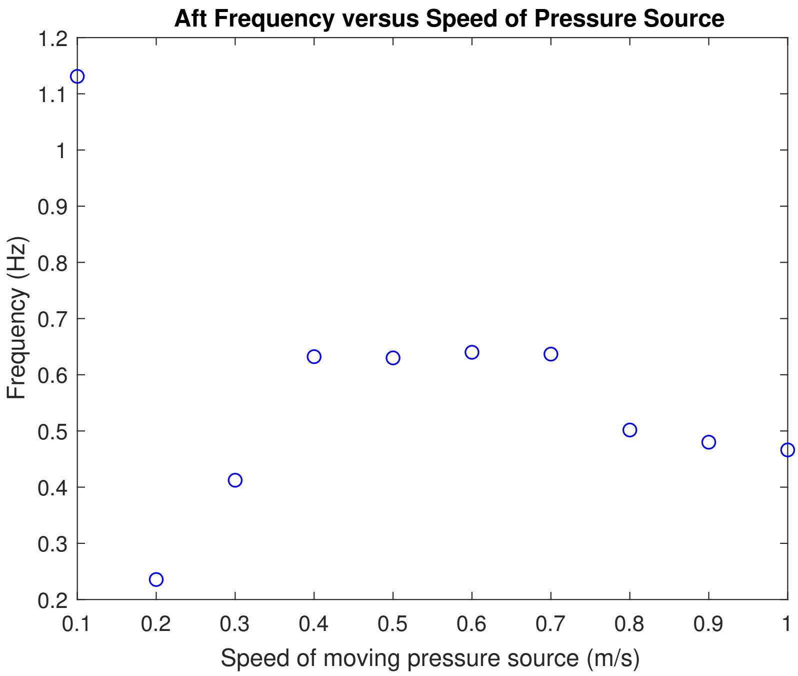

Figure 21: As the speed of the pressure source increases, the waves generated in the front (bow) of the pressure source have longer wavelengths as opposed to what is seen in Fig. 22

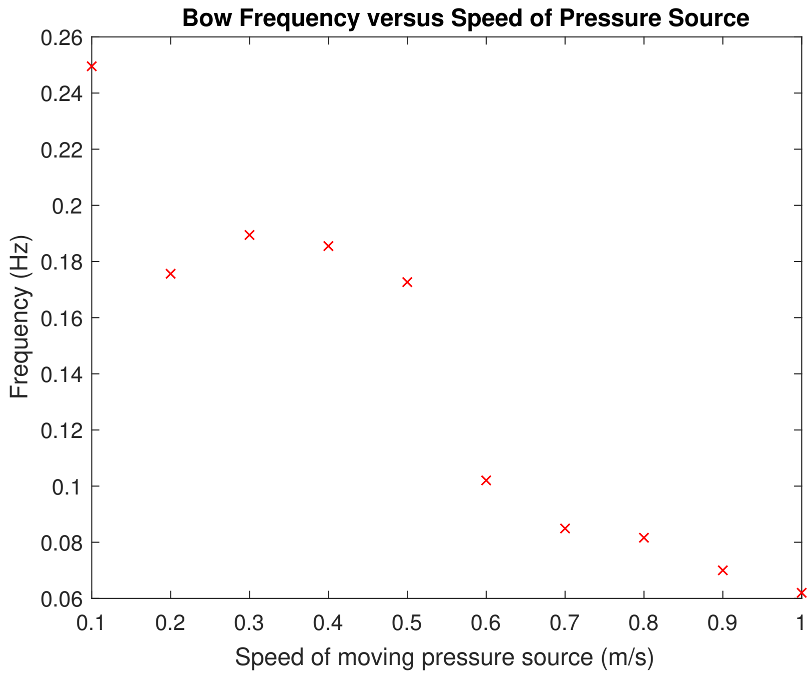

Figure 22: As the speed of the pressure source increases, the waves generated in the rear (aft) of the pressure source have shorter wavelengths as opposed to what is seen in Fig. 21

5 Uniformly Rotating Pressure Source in 3D

Extending the simulations from 2D to 3D space, test cases were carried out based on experimental observations and parameters. For the following simulations, a neumann boundary condition for free outflow is applied on the sides and top of the domain whereas a dirichlet boundary condition is imposed on the bottom of the domain to restrict flow from the bottom of the tank. In order to speed up the simulation process, an adaptive meshing scheme was implemented using in-built Basilisk functions. Using parameters similar to those seen in the previous 2D case, a pressure inter facial force was imposed on the liquid surface and variations in the angular speed and radius of circular trajectory were studied in accordance with experimental guidance.

Numerically speaking, the mesh was changed from a 'multi-grid' mesh to an 'octree' mesh as defined by Basilisk header files.

5.1 Static Pressure Source

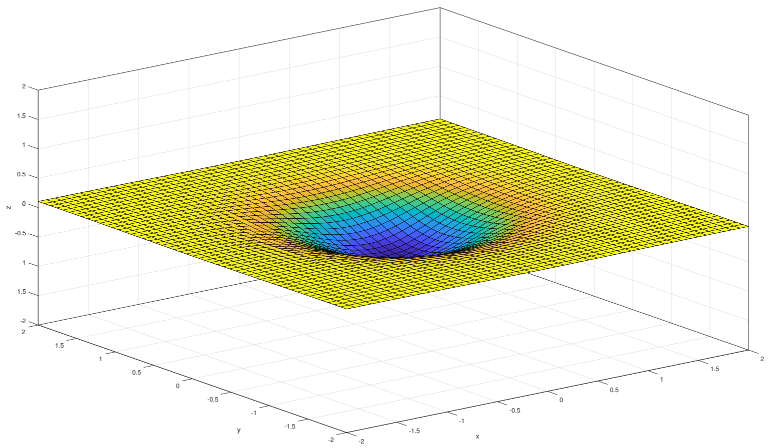

Figure 23: Full 3D simulation of a static inter facial pressure force on a high viscosity fluid showing conformity interface shape and shape of the applied force.

5.2 Rotating Pressure Source

Via guidance from experimental observations, the speed of rotation, radius of rotation and size of perturbation were simulated to trigger the formation of counter spirals. As seen in Fig. 24, the rotation of the pressure source perturbation induces the formation of counter spirals that radiate outwards from the trajectory of the pressure source.

From experiments we observe that:

1. The amplitude of the main and counter spirals are proportional to the speed of rotation of the pressure source.
2. The amplitude of the pressure source is proportional to the size of the perturbation of the pressure source. In this case, it is the width (or standard deviation) of the Gaussian pressure source.

To verify these observations, a temporal analysis needs to be carried out both in the frequency domain (Fourier space) and the time domain. A parametric study is underway.

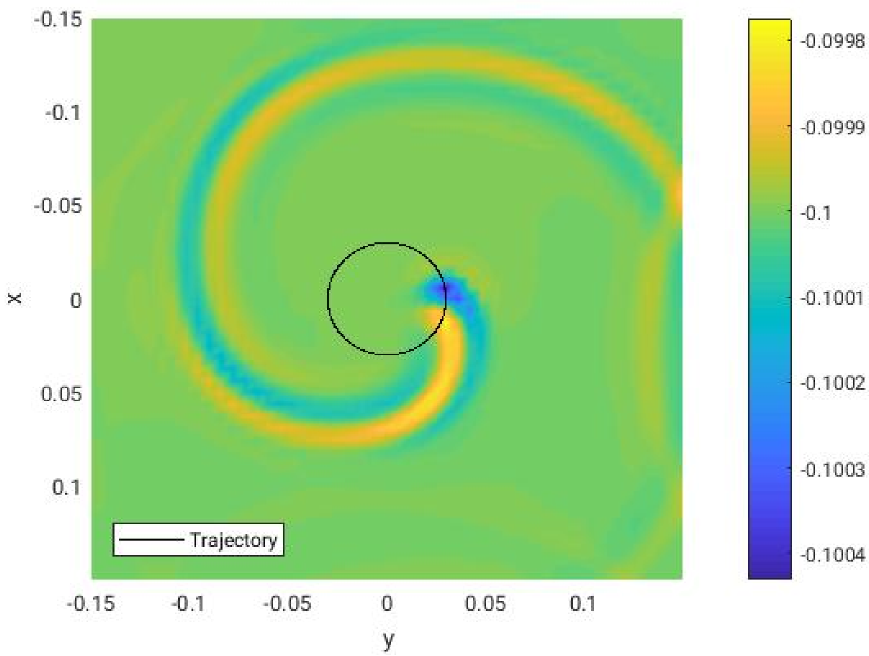

Figure 24: Full 3D simulation of a moving inter facial pressure force on fluid surface with main spirals clearly visible and the circle marking the trajectory of the pressure source.

5.3 Parametric Study

5.3.1 Effect of Speed of Rotation on Amplitude of Waves

From experimental observations, it is noted that the speed of rotation of the moving pressure source is proportional the amplitude of the wave generated. In Fig. 25, the simulations for a lower and a higher angular speed are visualized qualitatively. In the graph depicted in Fig. 26 it can be seen that this observation holds true up to a particular speed of rotation and then there exists a dip in the amplitude of waves generated.

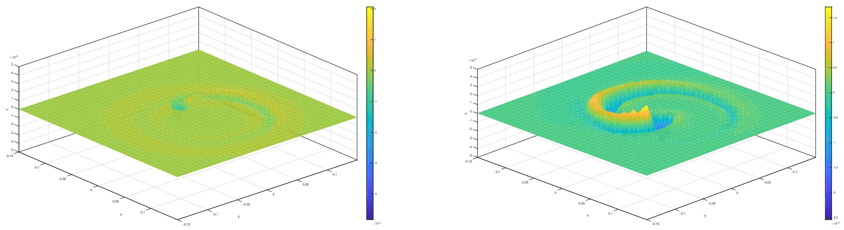

Figure 25: L-R: Pressure source with angular velocity of 1.8 rad/s; Pressure source source with angular velocity of 4.4 rad/s showing greater height of waves generated.

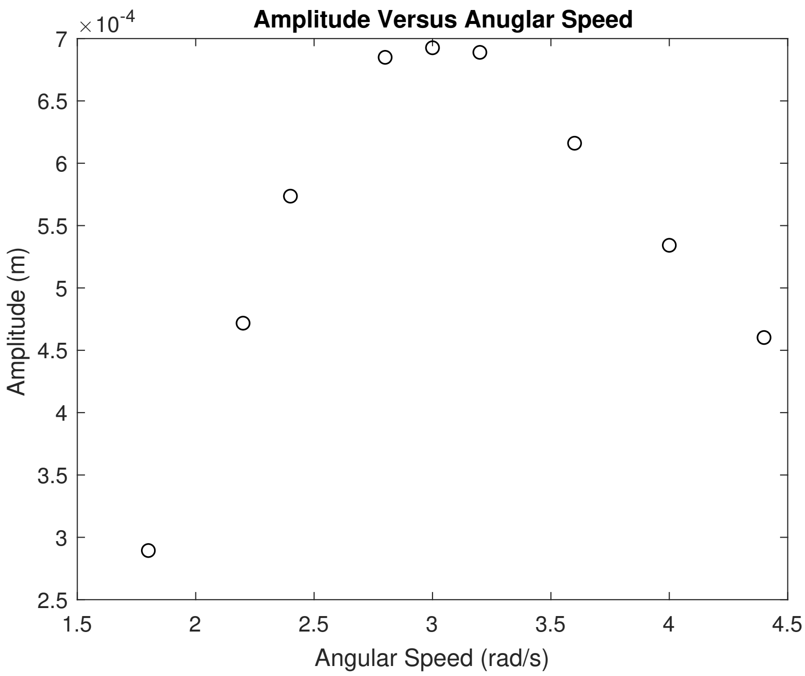

Figure 26: Change of wave amplitude with speed of moving pressure source.

5.3.2 Effect of Size of Perturbation on Amplitude of Waves

From experimental observations, the size of the perturbation, in our case, the standard deviation of the Gaussian pressure distributed source, affects the amplitude of the wave. From the simulations, the amplitude versus size of perturbation is shown in Fig. 27.

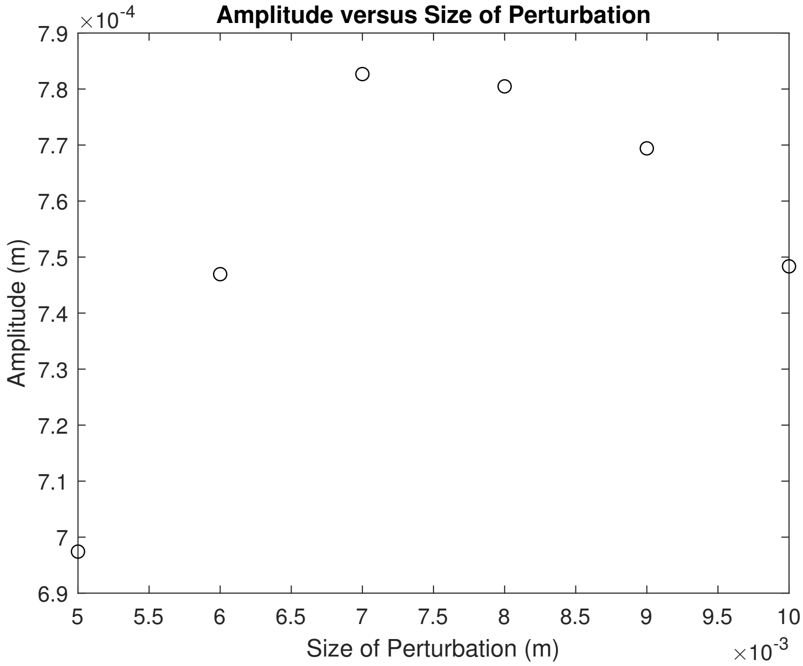

Figure 27: Change of wave amplitude with the size of moving Gaussian pressure source.

5.4 Comments and Conclusions

From Fig. 24 we do not see any counter spirals in the simulation that uses the Navier-Stokes equations i.e. full CFD. Only a single main spiral is visible. The following plausible explanations are presented below:

1. From Fig. 24 we do not see any counter spirals. In the experiment; the pressure source is a jet of air which falls in the turbulent regime. The following hand calculations based on experimental indications and indicate the presence of a turbulent regime within the jet of air.

$$U_{max} = \frac{6Q}{\pi(\frac{L}{2})^2} \tag{7}$$

$$Re = \frac{8Q}{L\nu} \tag{8}$$

$$Re = 1.55 \times 10^4 \tag{9}$$

   Eqn. 7 is obtained by assuming a parabolic distribution of air flow within the tube under a no-slip condition. For these calculations, the following values were used:

(a) Q, rate of airflow = $11.8 \mathrm{cm}^3/\mathrm{s}$,

(b) L, reference length, taken as the radius of the tube = 0.58mm,

(c) Mu kinematic viscosity of water = 0.0000010533 m/s,

This falls in the regime of turbulent flow whose physics is more unpredictable and is not taken into account in the simulations.

2. The magnitude of the counter spiral is much smaller than the main spiral, as seen in Fig. 28. Hence, there is a possible post processing issue that may cause the disappearance of the counter spirals.

3. The air jet moving along the surface of the water creates a shear force that creates a tangential component of the inter facial force that may be significant to the generation of the counter spirals.

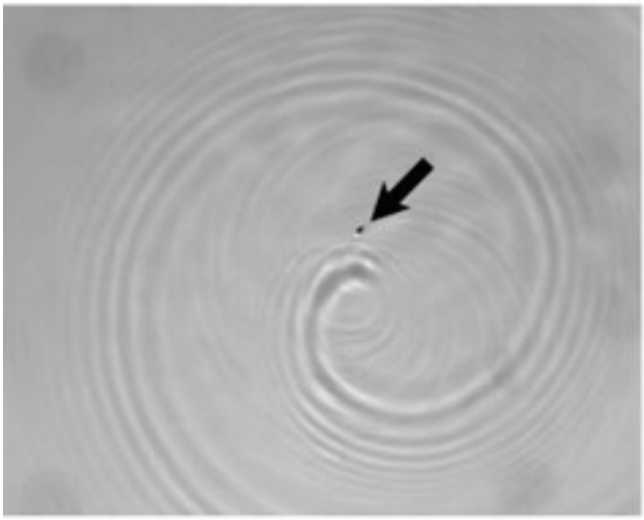

Figure 28: Actual pictures of the spiral wave (J. Voise et al., J. R. Soc. Interface, 2010)

6 Implementation of Code

6.1 Basilisk Implementation

To get started, one must follow the installation instructions found at http://basilisk.fr/src/INSTALL and install all requisite packages which will download all the header files including curvature.h, Navier-Stokes/centred.h, two-phase.h and other header files that are necessary to run the simulations.

Included with this package is the file curvature.h which includes comments in lines added by Kakadé. curvature.h is an original Basilisk file that was modified to apply inter-facial forces.

For the purposes of this simulation, 5 commented Basilisk C source code files were written:

1. To get the full dispersion relation titled 'dispersion.c'.

2. To apply a static pressure source on a water air interface for the Bond number analysis in 2D titled 'static2D.c'.
3. To apply a moving pressure source on a water air interface for the temporal analysis in 2D titled 'transient2D.c'.
4. To apply a static pressure source on a water air interface in 3D titled 'static3D.c'.
5. To apply a moving pressure source in uniform circular motion on a water air interface in 3D titled 'transient3D.c'.

Using the 'output facets' function, the height of the interface at different points on the mesh grid in a .txt file at each time step. To run the code successfully, copy these source codes to basilisk/src after installing Basilisk. Then, in the terminal use the command: 'qcc -O2 -Wall dispersion.c -o disp -lm' and then upon a successful compilation use './disp' to run the simulation. It may take a long time for the full 3D simulation to run.

6.2 MATLAB Implementation

All data from the Basilisk solver is imported into the MATLAB environment for the following non-exhaustive list of reasons:

1. MATLAB is more widely known by the scientific community than C/C++.
2. Ease of manipulation of data from time domain to frequency domain.
3. Parallel processing capability in post processing phase of analysis.

For the purposes of this simulation 5 commented MATLAB scripts were written:

1. To plot and study the dispersion relation titled 'MATLAB Dispersion Relation.m'
2. To visualize and study a static inter-facial force in 2D called 'MATLAB Static2D.m'
3. To conduct a bond number analysis on the above case called 'MATLAB Bond.m'
4. To visualize and study a transient inter-facial force in 2D called 'MATLAB Transient2D.m'
5. To visualize and study both the static and transient inter-facial force in 3D called 'MATLAB 3D.m'